Acta Crystallographica Section D
Biological Crystallography
ISSN 0907-4449

Structures of potent selective peptide mimetics bound to carboxypeptidase B

Marc Adler, Brad Buckman, Judi Bryant, Zheng Chang, Kieu Chu, Kumar Emayan, Paul Hrvatin, Imadul Islam, John Morser, Drew Sukovich, Christopher West, Shendong Yuan and Marc Whitlow*

Bayer HealthCare Pharmaceuticals, 2600 Hilltop Drive, PO Box 4099, Richmond, California 94804-0099, USA

Correspondence e-mail: marc_whitlow@sbcglobal.net

Received 31 August 2007
Accepted 8 November 2007

PDB References: carboxypeptidase B–inhibitor complexes, 2piy, r2piysf; 2piz, r2pizsf; 2pj0, r2pj0sf; 2pj1, r2pj1sf; 2pj2, r2pj2sf; 2pj3, r2pj3sf; 2pj4, r2pj4sf; 2pj5, r2pj5sf; 2pj6, r2pj6sf; 2pj7, r2pj7sf; 2pj8, r2pj8sf; 2pj9, r2pj9sf; 2pja, r2pjasf; 2pjb, r2pjbsf; 2pjc, r2pjcsf.

This article reports the crystal structures of inhibitors of the functional form of thrombin-activatable fibrinolysis inhibitor (TAFIa). *In vivo* experiments indicate that selective inhibitors of TAFIa would be useful in the treatment of heart attacks. Since TAFIa rapidly degrades in solution, the homologous protein porcine pancreatic carboxypeptidase B (pp-CpB) was used in these crystallography studies. Both TAFIa and pp-CpB are zinc-based exopeptidases that are specific for basic residues. The final development candidate, BX 528, is a potent inhibitor of TAFIa (2 n*M*) and has almost no measurable effect on the major selectivity target, carboxypeptidase N. BX 528 was designed to mimic the tripeptide Phe-Val-Lys. A sulfonamide replaces the Phe-Val amide bond and a phosphinate connects the Val and Lys groups. The phosphinate also chelates the active-site zinc. The electrostatic interactions with the protein mimic those of the natural substrate. The primary amine in BX 528 forms a salt bridge to Asp255 at the base of the S1′ pocket. The carboxylic acid interacts with Arg145 and the sulfonamide is hydrogen bonded to Arg71. Isopropyl and phenyl groups replace the side chains of Val and Phe, respectively. A series of structures are presented here that illustrate the evolution of BX 528 from thiol-based inhibitors that mimic a free C-terminal arginine. The first step in development was the replacement of the thiol with a phosphinate. This caused a precipitous drop in binding affinity. Potency was reclaimed by extending the inhibitors into the downstream binding sites for the natural substrate.

1. Introduction

Blood clots can be fatal because they may block coronary arteries and initiate a heart attack. This type of coronary event is known as acute myocardial infarction (AMI). Emergency treatment focuses on rapid dissolution of the clots (Anderson & Willerson, 1993; Lenderink *et al.*, 1995) using plasminogen activators such as recombinant tissue-type plasminogen activator (t-PA). These enzymes convert plasminogen to plasmin, a serine protease that degrades the fibrin matrix that underpins blood clots. This process is accelerated by the exposure of basic C-terminal residues on the partially degraded Aα-chains of fibrin that act as binding sites for both t-PA and plasminogen.

Under normal conditions, there is a balance between clot formation and clot dissolution. The activated enzyme thrombin-activatable fibrinolysis inhibitor (TAFIa) contributes to this balance by removing the C-terminal arginine and lysine residues from fibrin, thus reducing the formation of new plasmin and stabilizing the clot. TAFIa, a zinc-containing

Table 1
IC_{50} data.

Structures are shown in Fig. 1.

Compound†	PDB code	R_1	R_2	R_3	X	TAFIa (n*M*)‡	pp-CpB (n*M*)‡	CpN (n*M*)‡
BX 528	2piy	—	—	—	—	2.1	20	74000
(*R*)-**1**	1zg8	—	—	—	—	2.9	5.5	1700
(±)-**2**	2piz	—	—	—	—	8300	170	n.d.
(±)-**3**	2pj0	Cbz	*R*-iPr	$NHC(NH)NH_2$	O	160	8.1	7500
(±)-**4**	2pj1	Cbz	*R*-iPr	CH_2NH_2	O	7.9	9.7	46000
(±)-**5**	2pj2	Cbz	*R*-iPr	CH_2NH_2	C	5.3	12	24000
(±)-**6**	2pj3	$PhCH_2CH_2CO$	*R*-iPr	$NHC(NH)NH_2$	O	59	6.6	44000
(±)-**7**	2pj4	Cbz	*R*-cyclohexyl	$NHC(NH)NH_2$	O	190	13	30000
(±)-**8**	2pj5	Cbz	*R*-pentyl	$NHC(NH)NH_2$	O	930	15	30000
(±)-**9**	2pj6	$PhCH_2CH_2SO_2$	*R*-iPr	CH_2NH_2	C	15	49	53000
(±)-**10**	2pj7	$PhSO_2$	*R*-iPr	CH_2NH_2	C	15	17	>100000
(±)-**11**	2pj8	4-Ph-$PhSO_2$	*R*-iPr	CH_2NH_2	C	3.6	18	>100000
(±)-**12**	2pj9	Benzo-2,1,3-thiadiazole-4-SO_2	*R*-iPr	CH_2NH_2	C	5.4	12	90000
(±)-**13**	2pja	Cbz-Phe	*R*-iPr	$NHC(NH)NH_2$	C	6.1	2.2	3600
(±)-**14**	2pjb	CbzNCH(L-CH_2Ph)CH_2SO_2	*R*-iPr	CH_2NH_2	C	6.5	19	77000
(±)-**15**	2pjc	Cbz-Tyr	*R*-iPr	$NHC(NH)NH_2$	O	5.7	1.9	910

† The order of the compounds matches the PDB codes for the new structures. ‡ IC_{50} values are the mean of two or more experiments.

exopeptidase, is also known as plasma carboxypeptidase B, carboxypeptidase R and carboxypeptidase U. A variety of *in vitro* and *in vivo* studies (Redlitz *et al.*, 1995; Boffa *et al.*, 1998; Minnema *et al.*, 1998; Klement *et al.*, 1999; Refino *et al.*, 2000; Wang, da Cunha *et al.*, 2007) have demonstrated that a TAFIa inhibitor would be a useful adjunct to existing thrombolytic therapies in the treatment of AMI.

Our previous paper described a series of potent and selective thiol-based inhibitors of TAFIa that were developed with the aid of structure-based design (Adler *et al.*, 2005). X-ray crystallography was performed using porcine pancreatic carboxypeptidase B (pp-CpB) as a substitute for TAFIa. TAFI is not suitable for structural work because the activated form rapidly degrades in solution (Boffa *et al.*, 1998). pp-CpB is another zinc-containing exopeptidase that shares 47% sequence identity with TAFIa. The homology improves considerably in the presumptive active site, where there are only two conservative substitutions. Val203 and Leu247 in TAFIa are replaced by Leu and Ile in pp-CpB. Furthermore, pp-CpB is stable at room temperature and is available from commercial sources.

The inhibitors presented in our earlier work (Adler *et al.*, 2005) were structurally similar to L-arginine (**1** in Table 1; Fig. 1). Like arginine, each inhibitor had a free carboxylic acid connected to a guanidine by four C atoms. The α-amine of arginine was replaced by a mercaptomethyl group. X-ray crystallography revealed that the inhibitors bound in the S1′ site of pp-CpB. The thiol group chelated the active-site zinc, the guanidine formed a salt bridge to Asp255 and the free carboxylic acid formed hydrogen bonds to Arg145 and Asn144. The introduction of *meta*-substituted phenyl in place of the aliphatic chain significantly improved the selectivity of these compounds against other exopeptidases that cleave basic residues. Unfortunately, these compounds had poor pharmacokinetic properties. At the time, we believed that the free thiol reacted nonspecifically with other proteins. Subsequent research focused on replacing the thiol with an alternate group that would improve the pharmacokinetic properties of the compound and retain affinity for the active-site zinc.

Our optimized candidate, BX 528, is displayed in complex with pp-CpB (Fig. 2). BX 528 has an IC_{50} of 2 n*M* against human TAFIa (Wang, Zhao *et al.*, 2007), with almost no measurable activity against carboxypeptidase N (CpN). CpN is a critical enzyme in the complement system and the major selectivity target. This article will describe the development of BX 528 and present the series of structures that led to its discovery. The critical steps involved the replacement of hydrogen-bonding groups. These replacements provided significant improvements in potency and selectivity. Modification of the hydrophobic groups had less pronounced effects on the compound profiles.

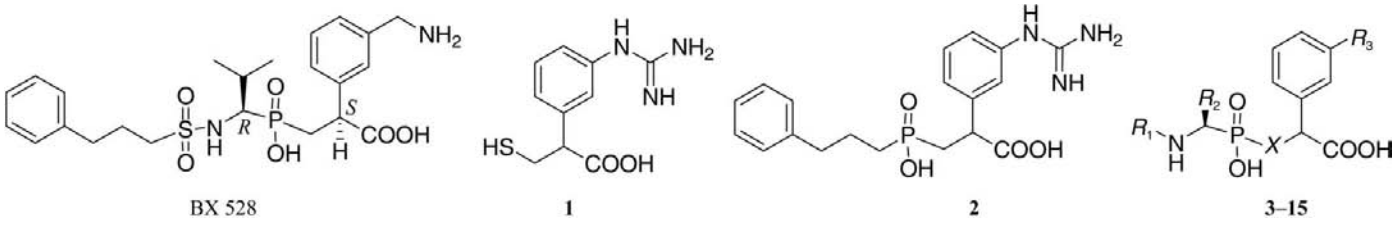

Figure 1
Covalent structures of inhibitors (see Table 1).

2. Experimental procedures

2.1. Compound synthesis

Compound **1** was synthesized as described previously by Adler *et al.* (2005). BX 528 and compounds **2**–**14** were synthesized as described previously by Wang, Zhao *et al.* (2007). BX 528 was prepared in a chirally pure form.

Our previous publication (Adler *et al.*, 2005) describes in detail the biochemical assays, protein-purification and crystallization, data-reduction and refinement protocols. We will briefly summarize the procedures below.

2.2. Enzyme-inhibition assays

The assays for inhibition of pp-CpB (Sigma, St Louis, Missouri, USA), thrombin/thrombomodulin-activated human plasma carboxypeptidase B (TAFIa) and carboxypeptidase N (CpN; Enzyme Research Laboratories, South Bend, Indiana, USA) were performed in 96-well or 384-well plates using adaptations of published protocols (Suzuki *et al.*, 1970; Hendricks *et al.*, 1986). The assays were preformed at ambient room temperature and pH 7.4 using hippuryl-L-arginine as a substrate. The amount of substrate hydrolyzed was determined by conversion of the product, hippuric acid, to a chromogen with cyanuric chloride/dioxane at pH 8.3. Following centrifugation, the absorbance of the supernatant was read at 382 nm. The IC_{50} values of the compounds were determined using the four-parameter equation from an eight-point dose-response curve, each compound being tested in duplicate.

2.3. Protein purification

Pp-CpB was obtained from Sigma (catalog No. C9584, St Louis, Missouri, USA) and purified on a TSK-GEL Phenyl 5PW column (catalog No. 14018, Tosohaas Biosciences, Montgomeryville, Pennsylvania, USA) using an ammonium sulfate gradient on an ÄKTA purification system (Amersham Pharmacia Biotech, Buckinghamshire, UK). Three pp-CpB peaks eluted from the Phe-HIC column. The large central peak was collected and DL-2-mercaptomethyl-3-guanidinoethylthiopropanoic acid was added to a final concentration of 1 m*M*. The pp-CpB was then buffer-exchanged on a 2.1 × 20 cm G25 Sepharose column into 10 m*M* Tris, 50 m*M* NaCl pH 7.0.

2.4. Crystallization

Each compound was dissolved in 10 m*M* Tris, 50 m*M* NaCl pH 7.0 and then added to the pp-CpB to a final concentration of 1.0 m*M*. The complex solutions were concentrated to between 25 and 40 g l^{-1}. The pp-CpB complex crystallizations

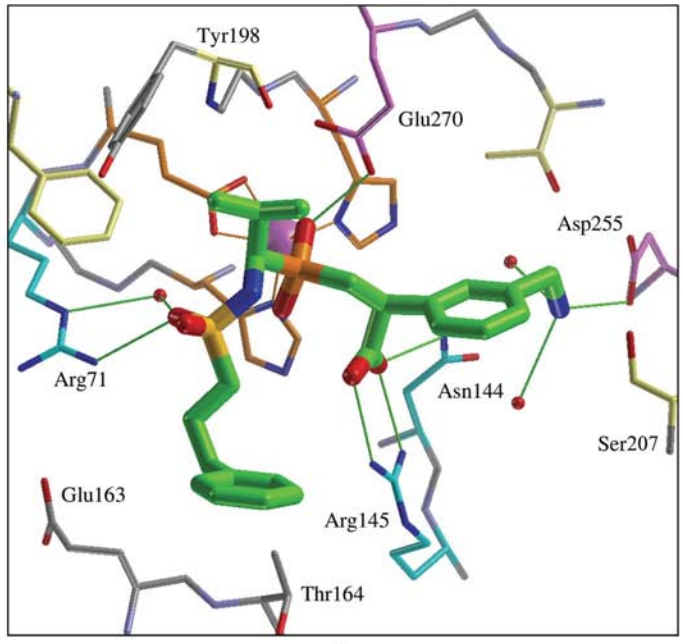

(*a*)

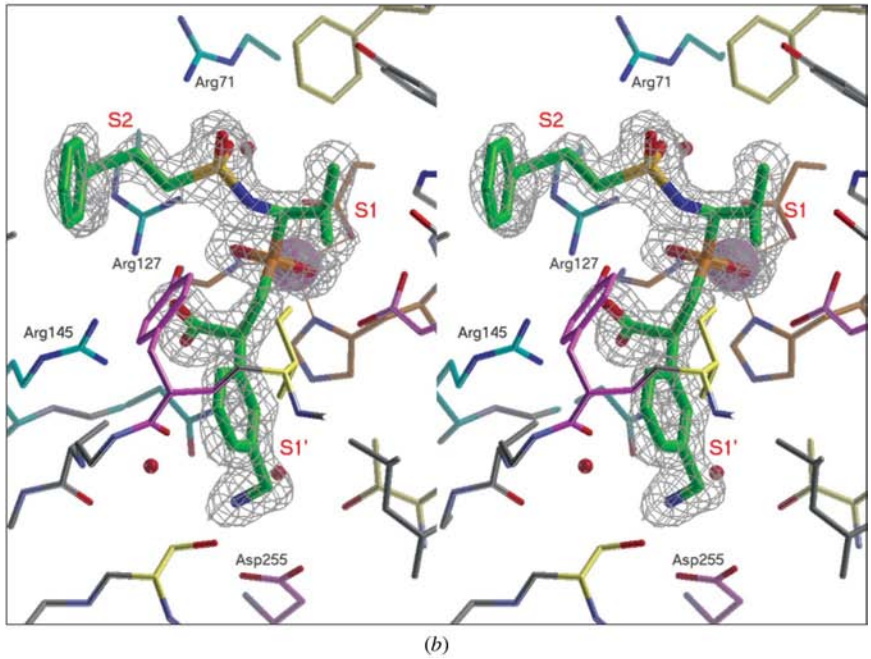

(*b*)

Figure 2
(*a*) BX 528 bound to pp-CpB, *A* subunit. Green lines depict hydrogen bonds. The loop containing Ile247 and Tyr248 forms a bridge over the S1′ binding site and obscures the view. This loop is omitted from most of the figures for the sake of clarity. Arg127, which forms the floor of the S2 pocket, was also omitted from most of the figures. (*b*) Divergent stereoview of the pp-CpB–BX 528 complex showing the electron density surrounding BX 528. The residues omitted in (*a*) are shown. The S1′, S1 and S2 subsites are labeled in red. The electron density was drawn for the $2F_o - F_c$ map contoured at 1σ using the 'blob' option in *XtalView* (McGee, 1992) with a 2 Å cutoff. Some stray density from neighboring atoms was removed by hand.

Table 2
Crystallographic data.

Compound	PDB code	Resolution (Å)	No. of reflections	Completeness (%)	Redundancy	R_{merge} (%)	$I/\sigma(I)$	Source†	Space group	Best subunit‡	Total atoms	R_{work}	R_{free}	R.m.s.d. bond (Å)	R.m.s.d. angle (°)	Average B factor (Å^2)
BX 528	2piy	1.43	158279	97.2	3.1	7.3	13.6	ALS 5.0.2	$P2_12_12_1$	*A* of 3	8349	0.181	0.203	0.009	0.8	16.8
2	2piz	1.60	112304	92.7	3.3	6.6	7.8	SSRL 7-1	$P2_12_12_1$	*A* of 3	7971	0.232	0.264	0.011	0.8	26.2
3	2pj0	1.65	88442	78.1	3.0	5.5	10.7	SSRL 7-1	$P2_12_12_1$	*C* of 3	7904	0.210	0.231	0.008	0.8	25.6
4	2pj1	1.64	105850	98.9	3.5	4.4	11.2	SSRL 9-1	$P2_12_12_1$	*C* of 3	8175	0.169	0.192	0.014	0.8	14.3
5	2pj2	1.95	63682	99.2	3.4	12.6	9.7	SSRL 9-1	$P2_12_12_1$	*C* of 3	7776	0.215	0.253	0.013	0.8	21.9
6	2pj3	1.64	102879	96.5	3.4	10.0	11.5	SSRL 9-1	$P2_12_12_1$	*C* of 3	8149	0.179	0.202	0.008	0.8	14.1
7	2pj4	2.00	49034	99.9	6.7	14.3	9.3	ALS 5.0.2	$P4_12_12$	*B* of 2	5235	0.215	0.265	0.017	0.9	17.7
8	2pj5	1.65	104480	98.8	3.5	6.7	9.5	SSRL 7-1	$P2_12_12_1$	*C* of 3	8234	0.172	0.195	0.008	0.8	15.2
9	2pj6	1.60	40559	99.6	7.2	5.5	19.2	ALS 5.0.2	$P2_12_12$	*A* of 1	2565	0.229	0.265	0.009	0.8	28.2
10	2pj7	1.77	84102	97.6	3.5	10.1	9.9	SSRL 11-1	$P2_12_12_1$	*A* of 3	7902	0.183	0.210	0.010	0.8	17.6
11	2pj8	1.70	95574	99.7	3.5	9.2	10.2	SSRL 11-1	$P2_12_12_1$	*C* of 3	7943	0.176	0.200	0.010	0.8	16.4
12	2pj9	1.56	54267	97.6	3.1	6.7	24.4	SSRL 11-1	$P2_12_12$	*A* of 1	2661	0.216	0.232	0.014	0.8	22.5
13	2pja	1.70	93217	96.2	3.5	8.7	7.2	SSRL 7-1	$P2_12_12_1$	*C* of 3	8065	0.189	0.219	0.010	0.8	21.3
14	2pjb	1.70	94505	98.0	3.2	6.8	12.8	Home	$P2_12_12_1$	*A* of 3	8240	0.174	0.200	0.010	0.8	16.6
15	2pjc	1.74	82012	92.3	3.4	7.5	12.9	SSRL 7-1	$P2_12_12_1$	*C* of 3	8022	0.179	0.209	0.006	0.8	24.9

† SSRL and ALS are acronyms for the Stanford Synchrotron Radiation Laboratory (Palo Alto, California, USA) and the Advanced Light Source (Berkeley, California, USA), respectively. ‡ This column lists the number of protein subunits in the asymmetric unit and the chain letter for the subunit that was used as the reference structure.

were prepared as hanging-drop vapour-diffusion experiments in Limbro 24-well plates. The reservoir contained between 0.15 and 0.30 *M* magnesium acetate, 0.1 *M* sodium cacodylate pH 6.5 and 12–22% polyethylene glycol 8000 (PEG 8000). The drop contained 2 µl pp-CpB complex and 2 µl reservoir solution. The drops were seeded with crystals from an earlier preparation of pp-CpB complexes.

2.5. Data collection

In general, each crystal was transferred to an equilibrated cryoprotection drop that contained 2 µl 20% polyethylene glycol 400 in the crystal's reservoir solution and 2 µl pp-CpB complex solution and held for 15 s. The crystal was then flash-cryocooled in liquid nitrogen and transferred to the X-ray goniostat. During data collection, the crystal temperature was maintained at 100 K. Most pp-CpB complex data sets were processed with *X-GEN* (Howard *et al.*, 1987). Experimental data were collected either from the Advanced Light Source, Berkeley, California, USA, at the Stanford Synchrotron Radiation Laboratory in Palo Alto, California or on our home source RU-300 with a Quantum-4 detector. Table 2 lists the data-collection statistics for each crystal.

2.6. Refinement

The pp-CpB complex structures were solved using direct replacement starting with the best available structure at the time. Simulated annealing (Brünger *et al.*, 1987) was used to refine the structure as the higher resolution data were introduced in successive steps. The inhibitors were fitted to the data once the resolution had been extended to 2.3 Å. Waters were added to the structure in all subsequent steps. The programs *X-PLOR* 3.1 (Brünger, 1993) and *XtalView* (McGee, 1992) were used in initial refinements of the structures. The final crystallographic refinements for all the structures were performed using *CNX*2005 (Brünger *et al.*, 1987; Accelrys Software Inc., San Diego, California, USA) and *PRODRG* was used to define the potentials for the inhibitors (Schüttelkopf & van Aalten, 2004). Further details for each structure are included in the headers of the files deposited in the PDB (http://www.pdb.org).

3. Results

Table 1 summarizes the key information in this report. It reports the chemical structures of the TAFIa inhibitors discussed in this paper (see also Fig. 1) and provides the PDB code for each structure. It also enumerates the measured IC_{50} for the inhibitors against three zinc-based exopeptidases: TAFIa, pp-CpB and CpN. Unless otherwise noted, the potencies listed in this report are the measured IC_{50} against TAFIa (Adler *et al.*, 2005). The table presents all the crystal structures that were generated during the development of phosphorus-based inhibitors of TAFIa. Some of the structures are not discussed in any detail within this manuscript. However, they may provide some useful information for the development of computational tools, such as scoring functions (Rajamani & Good, 2007). These structures are included in the tables for reference purposes.

3.1. The development of BX 528

TAFIa is a zinc-containing exopeptidase that cleaves basic residues from the C-termini of partially degraded fibrin. The substrate-binding pocket is divided into three subsites (Fig. 3*a*) that correspond to exposed residues on the C-terminus of the fibrin chain. The S1′ site binds the residue that is removed from the substrate. The residues that precede the cleavage site are numbered in reverse and the S1 residue becomes the new C-terminus. The preferences of the three binding sites are believed to be S1′, arginine and lysine; S1, small hydrophobic residues; S2, aromatic residues.

Initially, there were two structures of inhibitors bound to homologous proteins that guided our design efforts. These

structures delineate the binding interactions within the active site (Fig. 3*a*). The right side of the figure (S1′) shows the crystal structure of compound **1** from our last publication (Adler *et al.*, 2005; PDB code 1zg8). The left side shows a superposition of the S1 and S2 residues of carboxypeptidase inhibitor from potato (CPI) bound to carboxypeptidase A (Rees & Lipscomb, 1982; PDB code 4cpa). CPI inhibits TAFIa (110 n*M*), but has almost no measurable activity towards CpN (>33 000 n*M*). Furthermore, the structures of the S1 and S2 binding sites are nearly identical in CpA and pp-CpB and the contact residues are also conserved in TAFIa. Our goal was to develop novel inhibitors that combined the interactions from both **1** and CPI.

The first and most difficult step in the design processes was the replacement of the thiol group in **1** with an alternate zinc chelator, preferably a group that could be modified to extend into the S1 and S2 pockets (Fig. 3*a*). Our initial attempts with phosphate-based compounds produced inhibitors that had no measurable activity against TAFIa. Fig. 4(*a*) shows the structure of **2** (8300 n*M*) bound to pp-CpB. This was one of our first compounds without a thiol that had any measurable potency against TAFIa. Compound **2** binds the zinc through a single O atom in the phosphinate group (2.0 Å), completing the tetrahedral chelation sphere. The interaction mimics what was observed for the phosphonate groups in inhibitors of carboxypeptidase A (Kim & Lipscomb, 1991). A phenyl group extends into the S1 pocket of CpB. The activity of **2** is reduced by more than a 1000-fold when compared with that of the thiol-based inhibitor **1**. The loss of potency does not correlate with any detectable conformational strain. Instead, the lowered affinity is attributed to a weaker interaction with the zinc.

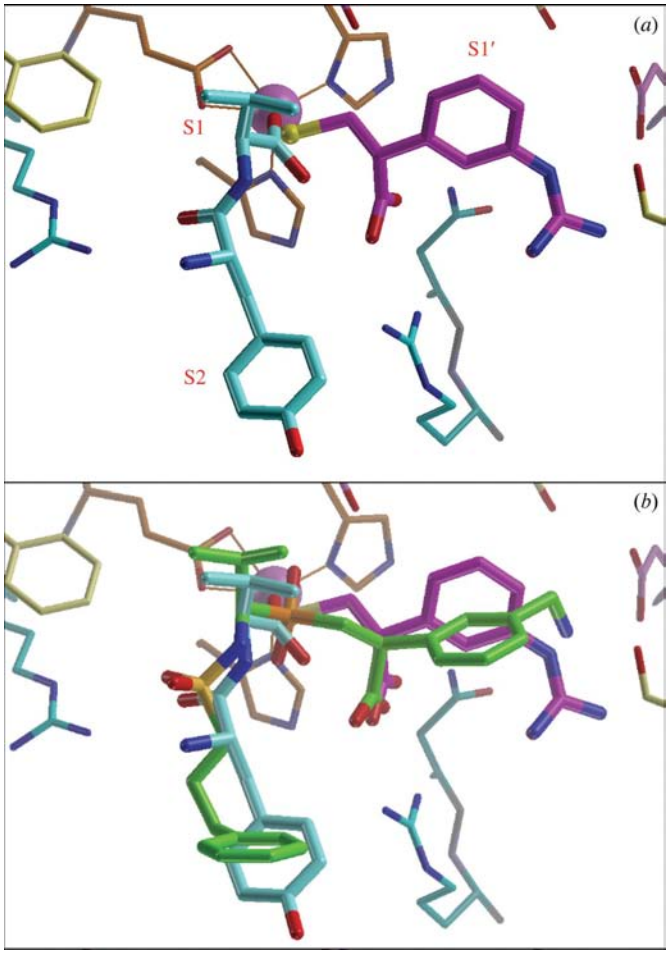

Figure 3
(*a*) A composite image made from three carboxypeptidase structures. The bound conformation **1** is shown in magenta (PDB code 1zg8; Adler *et al.*, 2005) and selected residues from carboxypeptidase inhibitor (CPI) are shown in cyan (PDB code 4cpa; Rees & Lipscomb, 1982). The protein itself is derived from the pp-CpB–BX 528 complex. (*b*) A superimposition of BX 528 (green) on **1** and CPI.

A major breakthrough came with the synthesis of **3** (160 n*M*; Fig. 4*b*). The left side of **3** was designed to mimic the S1 and S2 residues of CPI (Fig. 3*a*). The isopropyl and phenyl groups resemble the side chains of Val (S1) and Tyr (S2) residues, respectively. The phosphonate forms hydrogen bonds to the side chains of Arg127 (2.7 Å) and the catalytically active (Nau & Riordan, 1975) Glu270 (2.7 Å). Compound **3** uses a carbamate linker between the S1 and S2 pockets that maintains the same spacing as the peptide backbone. The carbamate carbonyl forms a hydrogen bond to Arg71 N^{η} (3.1 Å). There is also a water-mediated hydrogen bond from the carbonyl to Arg71 N^{ε} (3.0 Å). This conserved water is found in all of the structures from this template. The amide N atom forms a hydrogen bond to the phenol of Tyr248 (3.2 Å) and the aromatic side chain of Tyr248 is sandwiched between the two phenyl rings of the inhibitor (3.9 and 4.6 Å).

Compound **3** provided a well defined scaffold for further lead optimization. Subsequent work on this template explored the binding properties of the individual subsites. The implicit assumption was made that the compound's binding affinity is based on the sum of the individual parts. Although this assumption ignores confounding effects such as cooperativity, the approach simplified further optimization.

3.2. S1′ subsite

Originally, the S1′ substituents of our inhibitors were designed to mimic an L-Arg residue. TAFIa has a slight preference for Arg *versus* Lys (Tan & Eaton, 1995), but the enzyme will cleave both residues from the C-terminal ends of substrates (Myles *et al.*, 2003). An aminomethyl was substituted for the guanidine group in **3**, placing a lysine mimetic in the S1′ pocket. The resulting compound, **4** (8 n*M*), was 20 times more potent than its parent. The amine of **4** forms hydrogen bonds to Asp255 (2.8 Å), Ser207 (3.1 Å) and a water-mediated hydrogen bond to the backbone carbonyl group of Ala250. Other compounds in this series, such as BX 528 (Fig. 2), make two water-mediated hydrogen bonds (2.9 Å) to Ala250 and Thr268 and a salt bridge to Asp255 (2.7 Å). The methylene connector in **4** is more flexible than the corresponding group in **3**, which may improve the interaction with the protein. In addition, the lysine-based inhibitor **4** was less potent in CpN (24 000 n*M* *versus* 7000 n*M* for **3**) and the selectivity was improved by 70-fold.

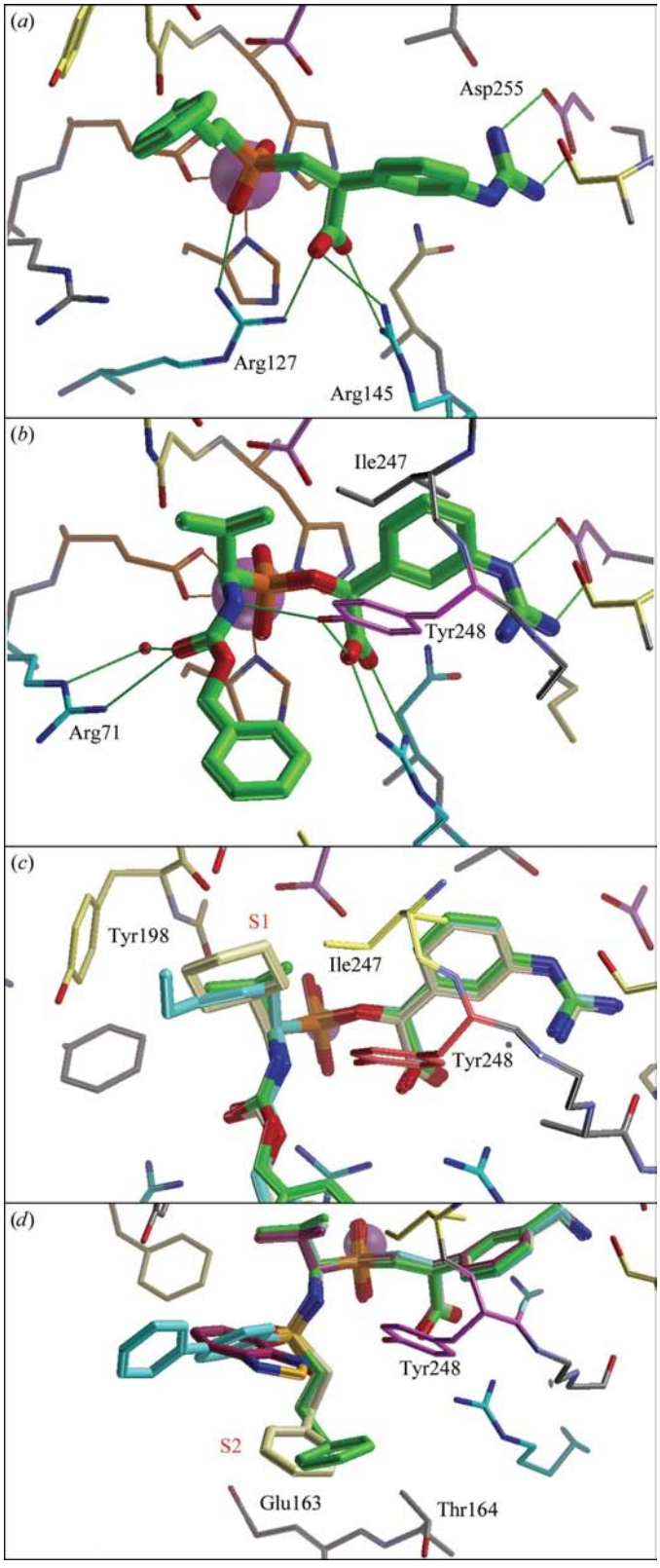

Figure 4
(*a*) **2** (8300 n*M*) bound to pp-CpB. (*b*) **3** (160 n*M*) bound to pp-CpB. The green lines show the network of hydrogen bonds formed by the carbamate group. These hydrogen bonds are also formed by the inhibitors when the carbamate is replaced by either an amide or a sulfonamide group. (*c*) Alternate S1 substituents: **3**, green (160 n*M*); **7**, ivory (190 n*M*); **8**, cyan (930 n*M*). (*d*) Alternate S2 substituents: BX 528, green (2 n*M*); **9**, ivory (7 n*M*); **11**, cyan (4 n*M*); **12**, dusty rose (5 n*M*).

The substitution of an aminomethyl (Lys) for the guanidine group (Arg) caused a conformational shift in the inhibitors. The S1′ phenyl of ring **4** is roughly perpendicular to the corresponding group in the guanidine-based inhibitors (Fig. 5). This shift had an interesting effect on the relative potencies in pp-CpB and TAFIa. The guanidine-based inhibitors are noticeably more potent towards pp-CpB than towards TAFIa, with an average ratio of 8.6 for the IC_{50} values (Table 1 and unpublished results using the geometric mean). In contrast, the amine-based inhibitors were slightly more potent against TAFIa (0.5 for the geometric mean of IC_{50} pp-CpB/IC_{50} TAFIa). The sequences of the two proteins indicate that the active sites are composed of the same residues; the only differences involve two aliphatic side chains that line the S1′ pocket (Fig. 5). Both of these residues face inward and can contact the S1′ substituent of the inhibitor. The data imply that these substitutions modulate the affinity through interactions with the phenyl ring in the S1′ pocket.

3.3. S1 subsite

Compound **3** has a valine-like group in the S1 pocket. The carbonyl of valine is replaced by a phosphonate, which may resemble the transition state (Park *et al.*, 2002). A large number of alternate side chains were synthesized and a limited number of crystal structures were obtained (**7** and **8** in Fig. 4*c*). There were no substantial improvements in potency and selectivity. Phosphonate and phosphinate had comparable activities and binding conformations (see **4** and **5**; Table 1). Eventually, the phosphonates were abandoned owing to our concerns about their stability.

3.4. S2 subsite and beyond

The carbamate linker in **3** and **4** replaces the amide bond between the S1 and S2 residues of CPI (Fig. 4*b*). The initial compounds included a carbamate because this group doubles as a protecting group for the nitrogen. Other linkers were also tested in this position. An amide linker demonstrated a twofold improvement in potency and selectivity (**6** *versus* **3** in Table 1). Ultimately, the best results were obtained using a sulfonamide linker between the S1 and S2 pockets (Fig. 2). BX 528 (2 n*M*) incorporates a sulfonamide linker and has almost no measurable activity in the CpN assay.

A number of alternate substituents were tried for the hydrophobic group in the S2 subsite (**9**–**12**; Fig. 4*d*). There were also several attempts to extend the compound into further downstream subsites (**13**–**15**). This approach had been successful with inhibitors of CpA (Kaplan & Bartlett, 1991; Kim & Lipscomb, 1991), but failed to show a consistent improvement with the sulfonamide-based inhibitors. The electron density was usually weak for the S2 hydrophobic group and it was difficult to accurately locate the aromatic rings in most structures. Furthermore, the *B* factors were usually elevated in this site. No consistent structure–activity relationships emerge from the work on the hydrophobic interactions in this site. A simple phenyl group attached by a linear propyl chain was used in BX 528.

3.5. The pp-CpB–BX 528 complex

The data for the pp-CpB–BX 528 complex extended to 1.43 Å resolution and the values of R and R_{free} for the final solution were 18.1% and 20.3%, respectively (Table 2). There were three copies of the protein in the asymmetric unit, which packed into the space group with unit-cell parameters $a = 66.9$, $b = 96.6$, $c = 136.0$ Å. The A and C subunits are free from any crystal contacts that would directly affect the active site. Tyr248 in the B subunit does come into contact (4.6 Å) with the Asn101 side chain in subunit C. This interaction seems to perturb the binding of the S2 moiety in some of the crystals.

Table 2 shows that the majority of crystals packed into space group $P2_12_12_1$. For each crystal, one subunit was selected as the best representation of the binding site. Selection was based on the clarity of the density for the S2 substituent and the absence of crystal-packing artifacts. The inhibitors generally adopted the same conformation in all three subunits. The notable exceptions to this were **13** and **15**. Both these inhibitors extend beyond the S2 site.

The electron density for BX 528 (Fig. 2) clearly defines the two chiral centers as R in the S1 site and S in the S1′. This matches the chirality of the naturally occurring L-amino acids Val and Lys. It is interesting to note that the S1′ chiral C atom of the thiol-based inhibitors (**1**; Adler *et al.*, 2005) was inverted compared with these inhibitors. The thiol-based inhibitors had a single carbon between the chiral center and the sulfur. The phosphinates had an additional atom inserted between the chiral center and the zinc chelator. The three bonds in the phosphinates maintain the same spacing as the natural substrates and preserve the original stereochemistry.

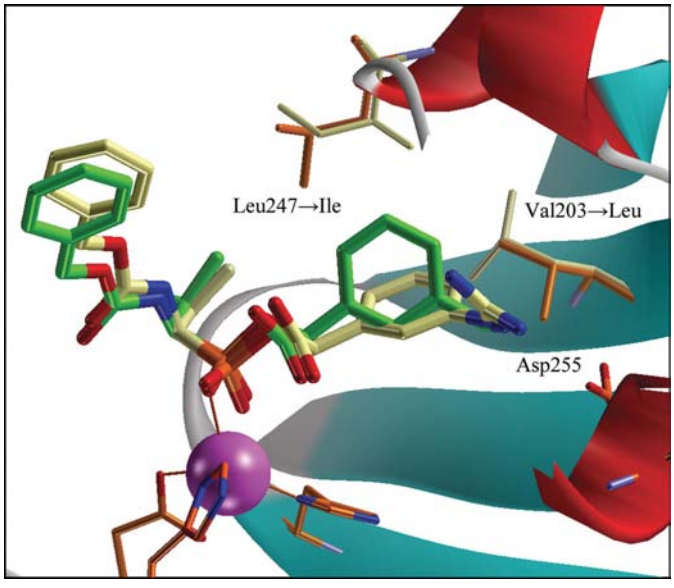

Figure 5
A comparison of the S1′ pocket of pp-CpB and TAFIa. Lysine mimetics such as **4** (green atoms) have a higher affinity for TAFIa. Arginine mimetics such as **3** (ivory) prefer pp-CpB. The residues that line the active site are conserved in both proteins, with two exceptions: Val203 and Leu247 (gold) in TAFIa are replaced by Leu and Ile (ivory) in pp-CpB. Val203 and Leu247 were modeled using the pp-CpB–**4** complex.

4. Discussion

BX 528 was designed to mimic the tripeptide Phe-Val-Lys. Fig. 3(*b*) compares the binding of BX 528 with that of carboxypeptidase inhibitor (CPI) which was used as a template in the design process. The sulfonamide substitutes for the peptide bond between Phe and Val, the phosphinate imitates the Val-Lys amide, the carboxylic acid replaces the free C-terminus and the free amine stands in for the N^{ε} atom of lysine. Fig. 2 shows the hydrogen bonds formed by these groups. The remainder of the inhibitor is either scaffolding or hydrophobic groups that imitate the original side chains of Phe-Val-Lys.

In our previous paper (Adler *et al.*, 2005), we proposed that the loop that covers the S1′ pocket, residues 245–249, may act as a flap that opens and releases the cleaved residue from the S1′ site. The deduction was based on the elevated B factors for this loop in structures in which the inhibitor did not extend beyond the S1′ pocket. The results presented are consistent with that conclusion and suggest a stepwise release of products from the enzyme. Fig. 4(*b*) indicates that the loop 245–249 is firmly held in place by residues that span both sides of the enzymatic cleavage site. Once the peptide bond has been cleaved, there are no strong interactions to hold the S1 and S2 residues in place and these residues are free to leave the active site. This exposes the 245–249 loop of CpB to the solvent and may destabilize the loop. This would in turn accelerate the release of the cleaved residue from the S1′ pocket. A direct proof of this hypothesis lies beyond the scope of our investi-

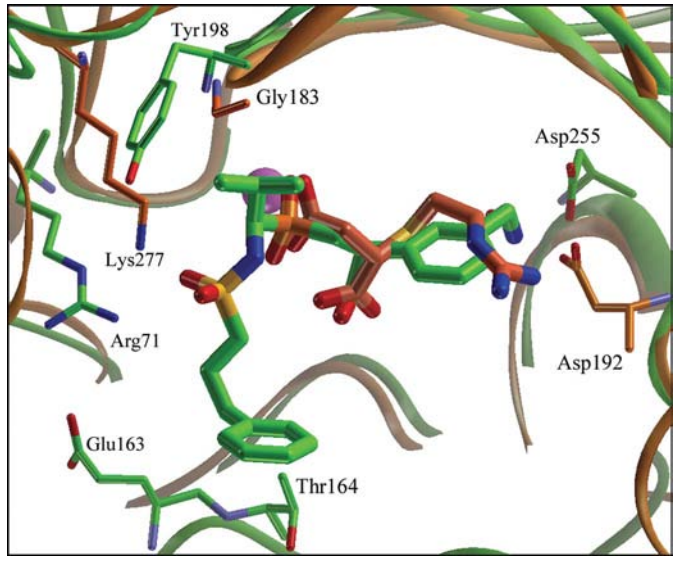

Figure 6
A ribbon diagram of the superimposed structures of pp-CpB–BX 528 (green) and CpD–GEMSA (orange and pink; PDB code 1h8l; Aloy *et al.*, 2001). Selected residues are shown for both proteins. These residues are conserved in TAFIa and CpN, respectively. Asp255 and Asp192 form a salt bridge with respective inhibitors, BX 528 and GEMSA. Arg71 hydrogen bonds to the S2 carbonyl in CpB. Presumably, Lys277 performs the same task in CpD. Tyr198 interacts with the isopropyl group in S1 and Glu163 and Thr164 contact the phenyl group in S2. The S1 and S2 pockets in CpD are more open and CpD does not have any residues that have the corresponding function.

gations. However, the hypothesis may help to explain why modifications to the S1 and S2 hydrophobic groups did not augment the potency of the template. The results suggest that weaker interactions with these groups may accelerate the release of product.

4.1. Selectivity of BX 528 against CpN

CpN is an important enzyme in removing anaphylotoxins such as C5a and C3a produced by the complement system (Willemse & Hendriks, 2006) and inhibition of this enzyme will result in undesirable side effects. CpN is another zinc-containing exopeptidase that shares TAFIa's specificity for C-terminal basic residues. Sequence analysis indicates that CpN and TAFIa have the same architecture. Valuable structural information about CpN can be deduced from the published structure of carboxypeptidase D (CpD) with the compound guanidinoethylmercaptosuccinic acid (GEMSA) bound in the active site (PDB code 1h8l; Aloy *et al.*, 2001). CpD shares 50% sequence identity with human CpN and the homology improves considerably in the active site.

Fig. 6 shows the superimposed structures of pp-CpB and CpD. The figure displays selected residues that are conserved in TAFIa and CpN. Presumably, the structural differences shown in Fig. 6 affect the substrate specificities of the two proteins. There are clear differences in the S1 and S2 sites of the two proteins. In pp-CpB, Tyr198 caps the top of the S1 subsite. The isopropyl group in BX 528 touches the aromatic ring of Tyr198 (3.7 Å; Fig. 6). In CpD, Tyr198 is replaced by Gly183 and the S1 pocket is more open. There are also important differences in the S2 site. The loop containing Glu163 and Thr164 defines the upper edge of the S2 pocket in pp-CpB. This loop is missing in CpD. These changes in CpD would leave the phenyl and isopropyl groups of BX 528 exposed to the solvent, thus reducing the positive interactions seen in CpB.

There are also important changes in the charged residues that line the active site. The sulfonamide O atom in BX 528 replaces the carbonyl group of the S2 peptide (Fig. 3*b*). Arg71 in pp-CpB forms a network of hydrogen bonds to this group. Presumably, Lys277 would have the same function in CpD since it is the only basic residue that is close. The side chain of Lys277 is shifted by more than 3 Å compared with Arg71 (Fig. 6) and this could affect inhibitor binding.

Finally, there are important differences between CpD and pp-CpB in the S1′ pocket that modulate selectivity. Asp255 in pp-CpB forms the critical salt bridge to the basic group of the inhibitor. CpD uses entirely different residues to form a salt bridge to the substrate (Fig. 6). The CpD–GEMSA structure indicates that the inhibitor binds to Asp192 and the backbone carbonyl of Tyr250 (the homologous residues in CpB are Ser207 and Tyr248.) Both these residues are closer to the surface than the corresponding hydrogen-bond acceptors in pp-CpB. The spatial differences change the conformation of the arginine-based inhibitors in each protein (see Fig. 6 in Adler *et al.*, 2005). The biochemical results indicate that the aminomethyl-based inhibitors do not readily bind to CpN (Table 1) even though these compounds should be long enough to reach the acidic group in the base of the S1′ pocket. The addition of the appropriate S1 and S2 groups effectively eliminates CpN binding.

We wish to thank Gary Phillips for his editorial guidance and useful insight. In addition, Iwona Minor of HKL Research Inc. (http://www.hkl-xray.com/) helped us analyze the images from two crystals where there were problems with twinning. The X-ray diffraction data were collected at either the Stanford Synchrotron Radiation Laboratory or the Advanced Light Source. The Stanford Synchrotron Radiation Laboratory is funded by the Department of Energy (BES, BER) and the National Institutes of Health (NCRR, NIGMS). The Advanced Light Source is a national user facility operated by Lawrence Berkeley National Laboratory on behalf of the US Department of Energy, Office of Basic Energy Sciences. The Berkeley Center for Structural Biology is supported in part by the Department of Energy, Office of Biological and Environmental Research and by the National Institutes of Health, National Institute of General Medical Sciences.

References

Adler, M., Bryant, J., Buckman, B., Islam, I., Larsen, B., Finster, S., Kent, L., May, K., Mohan, R., Yuan, S. & Whitlow, M. (2005). *Biochemistry*, **44**, 9339–9347.
Aloy, P., Companys, V., Vendrell, J., Avilés, F.-X., Fricker, L. D., Coll, M. & Gomis-Ruth, F. X. (2001). *J. Biol. Chem.* **276**, 16177–16184.
Anderson, H. V. & Willerson, J. T. (1993). *N. Eng. J. Med.* **329**, 703–709.
Boffa, M. B., Wang, W., Bajzar, L. & Nesheim, M. E. (1998). *J. Biol. Chem.* **273**, 2127–2135.
Brünger, A. T. (1993). *X-PLOR: A System for X-ray Crystallography and NMR*, version 3.1. New Haven: Yale University Press.
Brünger, A. T., Kuriyan, J. & Karplus, M. (1987). *Science*, **235**, 458–460.
Hendricks, D., van Sande, M. & Scharpe, S. (1986). *Clin. Chim. Acta*, **157**, 103–108.
Howard, A. J., Gilliland, G. L., Finzel, B. C., Poulos, T. L., Ohlendorf, D. H. & Salemme, F. R. (1987). *J. Appl. Cryst.* **20**, 383–387.
Kaplan, A. P. & Bartlett, P. A. (1991). *Biochemistry*, **30**, 8165–8170.
Kim, H. & Lipscomb, W. N. (1991). *Biochemistry*, **30**, 8171–8180.
Klement, P., Liao, P. & Bajzar, L. (1999). *Blood*, **94**, 2735–2743.
Lenderink, T., Simoons, M. L., Van Es, G.-A., Van de Werf, F., Verstraete, M. & Arnold, A. E. R. (1995). *Circulation*, **92**, 1110–1116.
McGee, D. E. (1992). *J. Mol. Graph.* **10**, 44–46.
Minnema, M. C., Friederich, P. W., Levi, M., von dem Borne, P. A., Mosnier, L. O., Meijers, J. C., Biemond, B. J., Hack, C. E., Bouma, B. N. & ten Cate, H. (1998). *J. Clin. Invest.* **101**, 10–14.
Myles, T., Nishimura, T., Yun, T. H., Nagashima, M., Morser, J., Patterson, A. J., Pearl, R. G., Lawrence, L. K. & Leung, L. L. (2003). *J. Biol. Chem.* **278**, 51059–51067.
Nau, H. & Riordan, J. F. (1975). *Biochemistry*, **14**, 5285–5294.
Park, J. D., Kim, D. H. & Kim, S. J. (2002). *J. Med. Chem.* **45**, 5295–5302.
Rajamani, R. & Good, A. C. (2007). *Curr. Opin. Drug Discov. Devel.* **10**, 308–315.
Redlitz, A., Tan, A. K., Eaton, D. L. & Plow, E. F. (1995). *J. Clin. Invest.* **96**, 2534–2538.
Rees, D. C. & Lipscomb, W. N. (1982). *J. Mol. Biol.* **160**, 475–498.

Refino, C. J., DeGuzman, L., Schmitt, D., Smyth, R., Jeet, S., Lipari, M. T., Eaton, D. & Bunting, S. (2000). *Fibrinolysis Proteolysis*, **14**, 305–314.
Schüttelkopf, A. W. & van Aalten, D. M. F. (2004). *Acta Cryst.* D**60**, 1355–1363.
Suzuki, S., Hachimori, Y. & Yaoeda, U. (1970). *Anal. Chem.* **42**, 101–103.
Tan, A. K. & Eaton, D. L. (1995). *Biochemistry*, **34**, 5811–5816.
Wang, Y. X., da Cunha, V., Vincelette, J., Zhao, L., Nagashima, M., Kawai, K., Yuan, S., Emayan, K., Islam, I., Hosoya, J., Sullivan, M. E., Dole, W. P., Morser, J., Buckman, B. O. & Vergona, R. (2007). *Thromb. Haemost.* **97**, 54–61.
Wang, Y. X., Zhao, L. *et al.* (2007). *Thromb. Haemost.* **97**, 45–53.
Willemse, J. L. & Hendriks, D. F. (2006). *Clin. Chim. Acta*, **371**, 124–129.